ADVANCED MATERIALS
www.advmat.de

Rapid Continuous Multimaterial Extrusion Bioprinting

Wanjun Liu, Yu Shrike Zhang, Marcel A. Heinrich, Fabio De Ferrari, Hae Lin Jang, Syeda Mahwish Bakht, Mario Moisés Alvarez, Jingzhou Yang, Yi-Chen Li, Grissel Trujillo-de Santiago, Amir K. Miri, Kai Zhu, Parastoo Khoshakhlagh, Gyan Prakash, Hao Cheng, Xiaofei Guan, Zhe Zhong, Jie Ju, Geyunjian Harry Zhu, Xiangyu Jin, Su Ryon Shin, Mehmet Remzi Dokmeci, and Ali Khademhosseini**

Recent advancements in bioprinting technologies have significantly improved our capability to fabricate artificial tissues and biomedical devices through bottom-up assembly of biomaterials, biomolecules, and cells.[1] The spatial arrangement of distinctive components in the resulting constructs is of critical importance to achieve tissue and device functions. The bioprinting technologies, including extrusion-based printing,[2] laser-based printing,[3] inkjet-based printing,[4] acoustic encapsulation,[5] and valve-based printing,[6,7] have provided robust platforms that allow for controlled deposition of 3D constructs with predefined patterns. Among these different methods, extrusion-based bioprinting is one of the most popular methodologies presently used due to its compatibility with various bioinks and ease of operation.[8]

A typical extrusion bioprinter is composed of three units: a reservoir (e.g., syringe) that contains the bioink, a printhead through which the bioink is ejected from the reservoir, and a receiving stage where the deposited bioink is collected.[9] The printhead, the stage, or both, may be motorized to achieve elaborate control of bioprinting based on precisely designed patterns. Nevertheless, most of the current modalities are limited to the use of a single bioink during each deposition process,

W. Liu, Dr. Y. S. Zhang, M. A. Heinrich, F. De Ferrari, Dr. H. L. Jang, S. M. Bakht, Prof. M. M. Alvarez, Dr. J. Yang, Dr. Y.-C. Li, Dr. G. Trujillo-de Santiago, Dr. A. K. Miri, Dr. K. Zhu, Dr. P. Khoshakhlagh, G. Prakash, H. Cheng, X. Guan, Z. Zhong, Dr. J. Ju, G. H. Zhu, Dr. S. R. Shin, Dr. M. R. Dokmeci, Prof. A. Khademhosseini
Biomaterials Innovation Research Center
Division of Engineering in Medicine
Brigham and Women's Hospital
Harvard Medical School
Cambridge, MA 02139, USA
E-mail: yszhang@research.bwh.harvard.edu; alik@bwh.harvard.edu

W. Liu, Dr. Y. S. Zhang, M. A. Heinrich, F. De Ferrari, Dr. H. L. Jang, S. M. Bakht, Prof. M. M. Alvarez, Dr. J. Yang, Dr. Y.-C. Li, Dr. G. Trujillo-de Santiago, Dr. A. K. Miri, Dr. K. Zhu, Dr. P. Khoshakhlagh, G. Prakash, H. Cheng, X. Guan, Z. Zhong, Dr. J. Ju, G. H. Zhu, Dr. S. R. Shin, Dr. M. R. Dokmeci, Prof. A. Khademhosseini
Harvard-MIT Division of Health Sciences and Technology
Massachusetts Institute of Technology
Cambridge, MA 02139, USA

W. Liu, Prof. X. Jin
Key Laboratory of Textile Science and Technology
College of Textiles
Donghua University
Shanghai 201620, China

Dr. Y. S. Zhang, Dr. P. Khoshakhlagh, Dr. S. R. Shin, Dr. M. R. Dokmeci, Prof. A. Khademhosseini
Wyss Institute for Biologically Inspired Engineering
Harvard University
Boston, MA 02115, USA

M. A. Heinrich
MIRA Institute of Biomedical Technology and Technical Medicine
Department of Developmental BioEngineering
University of Twente
Enschede 7500AE, The Netherlands

F. De Ferrari
Department of Electronics and Telecommunications
Politecnico di Torino
Torino 10129, Italy

S. M. Bakht
COMSATS Institute of Information and Technology
Islamabad 45550, Pakistan

Prof. M. M. Alvarez, Dr. G. Trujillo-de Santiago
Microsystems Technologies Laboratories
Massachusetts Institute of Technology
Cambridge, MA 02139, USA

Prof. M. M. Alvarez, Dr. G. Trujillo-de Santiago
Centro de Biotecnología-FEMSA
Tecnológico de Monterrey at Monterrey
Monterrey, Nuevo León, CP 64849, Mexico

Dr. J. Yang
School of Mechanical and Chemical Engineering
University of Western Australia
Perth, WA 6009, Australia

Dr. K. Zhu
Department of Cardiac Surgery
Zhongshan Hospital
Fudan University
Shanghai 200032, P. R. China

Dr. K. Zhu
Shanghai Institute of Cardiovascular Disease
Shanghai 200032, P. R. China

G. H. Zhu
Department of Polymer Engineering
University of Akron
Akron, OH 44325-0301, USA

Prof. A. Khademhosseini
Department of Bioindustrial Technologies
College of Animal Bioscience and Technology
Konkuk University
Seoul 143-701, Republic of Korea

Prof. A. Khademhosseini
Department of Physics
King Abdulaziz University
Jeddah 21569, Saudi Arabia

DOI: 10.1002/adma.201604630

rendering it difficult to achieve bioprinting of sophisticated compositional structures. Several techniques have recently been advanced to overcome this limitation in an effort to improve the capacity of bioprinters to extrude more than a single bioink. For example, a simple mixing device was fixed onto the printhead for printing of two materials.[10–12] In addition, multimaterial bioprinting was realized by incorporating multiple separate printheads on a bioprinter, where mechanical co-registration of the printheads achieved the deposition of selected inks at desired locations.[13–16] Despite their potential in scaling up to a larger number of materials, the deposition speed of this technique would inevitably be reduced as more nozzles are added, since fast switching among different channels and simultaneous injection of bioinks can hardly be achieved.

Here, we report a multimaterial extrusion bioprinting platform that is capable of extruding multiple coded bioinks in a continuous manner with fast and smooth switching among different reservoirs for rapid fabrication of complex (tissue) constructs. This paper provides a proof-of-concept demonstration by mounting a single printhead consisting of a bundle of seven equal-sized capillaries, each connected to a unique bioink reservoir that could be individually actuated by digitally controlled pneumatic pressure. The ejection process, when synergized with the movement of the motorized stage, allows for rapid deposition of 2D patterns and 3D architectures composed of multiple desired bioinks in a spatially defined manner, at a speed an order of magnitude faster than most existing nozzle-based bioprinting modalities. We further demonstrated the capability of our rapid continuous multimaterial bioprinter to generate miniaturized cell-laden constructs containing several types of cells, as well as its potential to fabricate gradient structures, and prototype multicomponent bioelectronics, using a broad range of bioinks from shear-thinning to conductive biomaterials. The proposed technology is likely to advance the field of extrusion bioprinting by offering strong capacity in printing speed and continuity, which is compatible with a wide variety of bioinks. Most of all, our 3D bioprinting platform may be conveniently extended to a large numbers of bioinks necessary for engineering highly complex functional biomaterials, tissues, and devices in the future.

Unlike conventional multinozzle bioprinters, which typically require mechanical switching among the physically separated nozzles to deposit multiple bioinks, our bioprinter is able to continuously eject different types of bioinks in both individual and simultaneous modes. The bioprinter consists of a Cartesian robotic stage and an array of bioink reservoirs routed to a single printhead containing seven bundled channels with equal sizes (**Figure 1**A–D and Figure S1 and S2, Supporting Information). The dispensers are pneumatically driven and fed by compressed gas through valves (Figure 1C). Digital tuning of the extrusion is achieved using a program integrated with the bioprinter to individually (or simultaneously) switch on/off desired valve(s) and command the dispensing patterns (Figure 1B,C). The controllers for both the valves and the motorized stage are programmed to synchronize the actuation of the valves and the movement of the stage. The adjustment of the pneumatic pressure and valve gating duration allows the dispersion of various bioinks with different viscosities. As such, this bioprinter can print up to seven materials and rapidly switch among materials from different channels, without needing to physically change the nozzles.

Here shear-thinning bioinks formulated by a suspension of synthetic nanosilicates in water were employed for bioprinting.[17,18] Detailed investigations of the rheological properties and the printing performance of the silicate bioinks can be found in Figure S3–S6 in the Supporting Information. It should be noted that the 5% nanosilicate bioink was chosen as the optimal formulation that possessed proper shear-thinning properties, and was thus used to bioprint various 3D constructs. As an example, we programed the bioprinter to deposit bioinks dyed in seven different colors with increasing numbers of colors after each switch (Figure 1E,F and Movie S1 in the Supporting Information). The bioprinting process was continuous, and the printed microfibrous structure maintained its three-dimensionality consisting of an array of spatially well-defined bioinks (Figure 1G). The seven bioinks could also be individually deposited via a continuous printing process (Movie S2, Supporting Information), where no noticeable switching delays were observed between adjacent materials (Figure S7, Supporting Information).

We next printed a series of microfibrous 2D patterns to demonstrate the capability of our bioprinter for continuous extrusion of multiple materials in well-defined manners. Each of the seven bioinks could be continuously printed in equivalent lengths along the direction of the individual microfibers, with equal or incremental spacing between the adjacent lines (Figure S8A,B, Supporting Information). Alternatively, the spacing between the adjacent microfibers could be maintained constant while continuous segments within individual lines were printed with decreasing lengths (Figure S8C, Supporting Information), or both parameters might be altered simultaneously during the bioprinting process (Figure S8D, Supporting Information). We further printed an array of microfibers composed of increments of one to seven materials along the direction of individual lines (Figure S8E, Supporting Information). Printing of these various patterns demonstrated the capability of our platform to continuously deposit any desired type and number of bioinks on demand. The different materials could also be printed in perpendicular directions, to achieve hierarchical architecture while still maintaining a clear separation of the deposited bioinks (Figure S8F–J, Supporting Information). The printed multimaterial microfibers could be designed to fuse into a single piece of structure when the spacing between the microfibers was reduced to match their width (Movie S3, Supporting Information). The printed microfibers joined each other and formed a cohesive piece of monolayer slab containing seven distinct but continuous segments along the direction of microfiber deposition. This ability to create fused larger-scale constructs allowed us to print more sophisticated patterns composed of multiple bioinks, which has hardly been possible using existing multiprinthead systems.[13] Our continuous multimaterial bioprinter has shown unparalleled power in overcoming this inability by depositing multiple types of materials in precisely programmed arrangements at much improved fabrication speed.

It is estimated that our continuous multimaterial bioprinter features much faster fabrication speed than most existing multinozzle systems. For a typical multinozzle printer, the switch

Adv. Mater. **2016**,
DOI: 10.1002/adma.201604630

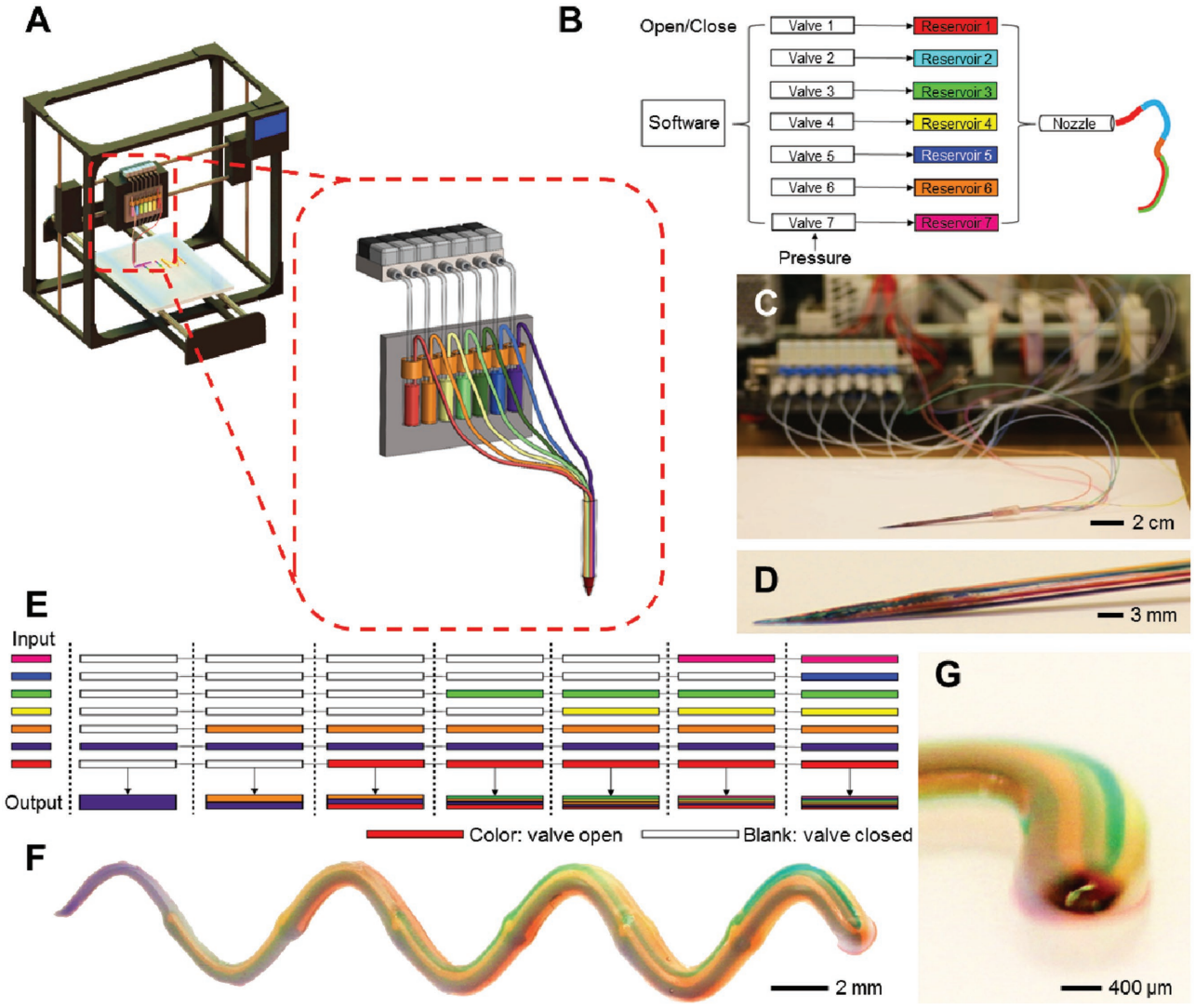

Figure 1. Design of the digitally tunable continuous multimaterial extrusion bioprinter. A,B) Schematics showing the design of the seven-channel printhead connected to reservoirs that are individually actuated by programmable pneumatic valves. C,D) Photographs showing the setup of the Festo valves and printhead. E) Schematic of a sample code for continuous bioprinting of a single serpentine microfiber consisting of one to seven bioinks. F) Photograph showing the printed microfiber. G) Side view of the end of the microfiber indicating the 3D volume containing seven individually segmented bioinks. Printing conditions: 5% nanosilicate aqueous suspension dyed in seven different colors, printhead moving speed = 400 mm min^{-1}, pneumatic pressure = 50 psi.

time between nozzles averages 4–20 s.[14,16] In comparison, our continuous bioprinting platform requires nearly no gap in such switching processes. In analyzing our fabrication procedure where we printed 15 lines each composed of seven bioinks for two layers (and thus 180 switches in total, Movie S3, Supporting Information), while our continuous bioprinter spent only 256 s for the entire printing process (at a speed of 400 mm min^{-1}), a conventional multinozzle printer will consume an additional time of 720–3600 s simply devoted to physical nozzle switching and results in a total printing time of 976–3856 s, if the patterns are deposited in the same manner. Therefore, our continuous multimaterial bioprinter could achieve a speed up to 15 times faster than those of the existing nozzle-based platforms. Although the numbers in this comparison is not completely accurate due to the different materials used in the literature and in our case, it is still indicative of the potential superior capacity of our multimaterial bioprinter to deposit several bioinks than existing multinozzle platforms. The advantage of our continuous multimaterial extrusion printing system in terms of the biofabrication speed would become much more pronounced as the number of materials and the complexity of the printouts are increased. These unique features of our bioprinter have significantly promoted the current level of automation and speed among existing nozzle-based bioprinting techniques.[11,14,19] It should be noted that, the present system is readily expandable to as many bioinks as needed by simply increasing the number of pneumatically driven valves and reservoirs, thus affording us the possibility to rapidly generate complex constructs while simplifying instrumentation.

We next demonstrated the capability of our continuous multimaterial bioprinter to produce complex 3D constructs.

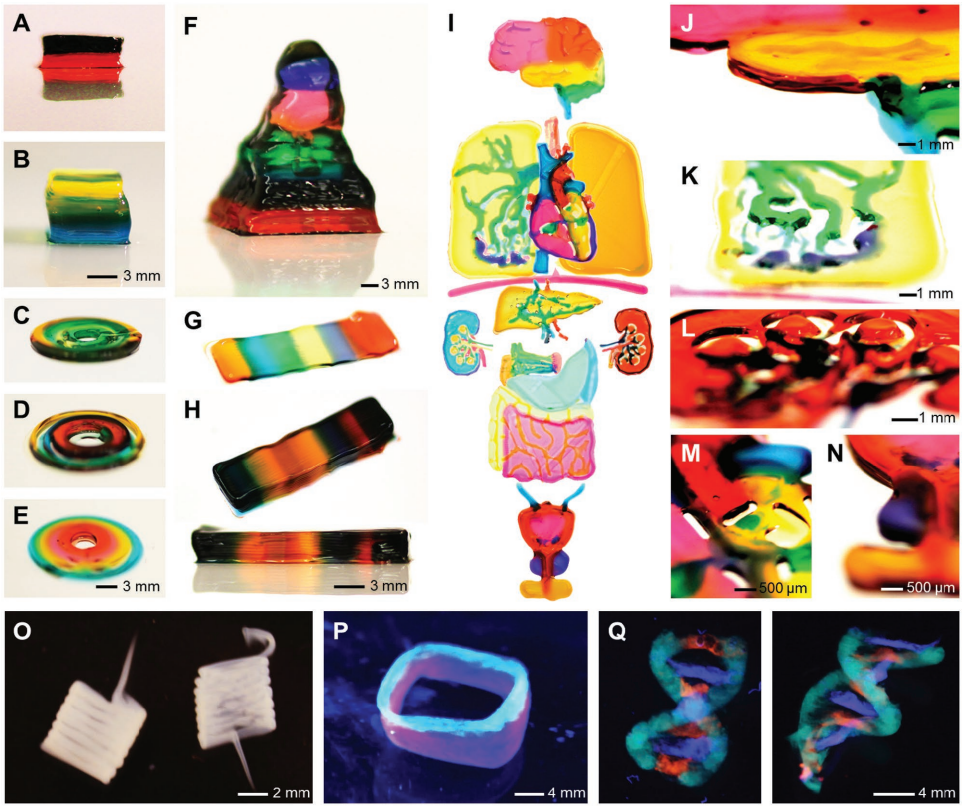

Figure 2. Multimaterial bioprinting of 3D constructs. A,B) Bioprinting of dual- and triple-layered cuboid blocks. C–E) Bioprinting of blood-vessel-like structures (transverse plane) containing dual, triple, and quadruple materials. F) Bioprinting of a pyramid containing seven layers of different bioinks. G,H) Bioprinting of three- and ten-layered blocks with continuous segments of seven different bioinks. I) Bioprinting of human organ-like constructs from multiple bioinks, including brain, lung, heart, liver, kidneys, pancreas, stomach, small/large intestines, bladder, and prostate. The organ-like constructs were individually printed, photographed, and stitched together in the same image at relative locations as those in the human body. J–N) Side view of selected organ-like constructs indicating their 3D nature: J) brain, K) lung vasculature, L) kidney, M) left atrium of heart, N) bladder/prostate. The organ-like structures were not printed to scale to each other. A–N) Printing conditions: 5% nanosilicate aqueous suspension dyed in seven different colors, printhead moving speed = 400 mm min^{-1}, pneumatic pressure = 50 psi. Embedded bioprinting of O) free-form coils (printing conditions: 20% PEGDA, 2% alginate, and 0.5% PI extruded in 23% Pluronic aqueous solution; printhead moving speed = 100 mm min^{-1}, pneumatic pressure = 30 psi), P) dual-layer hollow tube, and Q) DNA helix in front and side views. P,Q) Printing conditions: 2% alginate dyed in different colors extruded in 23% Pluronic aqueous solution containing 0.05% $CaCl_2$; printhead moving speed = 100 mm min^{-1}, pneumatic pressure = 30 psi.

Simple cubes composed of 2 and 3 bioinks (**Figure 2**A,B) and ring-shaped blocks containing 2, 3, and 4 bioinks were readily printed (Figure 2C–E). Constructs containing all seven bioinks could also be fabricated in different shapes, such as a pyramid (Figure 2F), a three-layer stripe (Figure 2G), and a ten-layer stripe (Figure 2H). We further designed sophisticated 3D patterns and printed a set of structures resembling human organs, including brain, lung, heart, liver, kidneys, pancreas, gastrointestinal system, and bladder. Each organ-like structure contained four to seven bioinks, according to the requirements of local structures, and each was individually printed (Figure 2I and Movie S4–S7, Supporting Information). Only one to three layers of the bioinks were deposited in these examples due to the significant amount of time required for printing these structures of relatively large scales. The bioprinting processes were rapid, and the transition among different bioinks was smooth. The printed organ-like constructs were stable, and the demarcation among adjacent materials was clear (Figure 2J–N, and Figure S9, Supporting Information). Our multimaterial bioprinter was also compatible with the embedded bioprinting technique.[7] Using a modified printhead with extended length, we were able to directly generate free-form shape of polyethylene glycol-diacrylate (PEGDA)/alginate coils in a Pluronic hydrogel followed by photo-crosslinking and retrieval after liquefying the supporting matrix (Figure 2O). Similarly, free-form alginate shapes composed of multiple bioinks, such as a dual-layer hollow tube (Figure 2P) and a DNA double helix-like structure (Figure 2Q), could be obtained with our continuous multimaterial bioprinter.

The developed rapid continuous multimaterial bioprinter should be able to generate hierarchical structures and patterns suitable for various applications in biomedicine. We subsequently demonstrated the capability of the bioprinter in engineering complex cell-laden organs and depositing prototype bioelectronic circuits. While these demonstrations are preliminary with limited resolution and functional assays, we primarily aimed to validate the concept of our continuous multimaterial extrusion bioprinting in the current work.

Adv. Mater. **2016**,
DOI: 10.1002/adma.201604630

Among the various photo-crosslinkable hydrogels available, gelatin methacryloyl (GelMA) has been frequently used as a bioink due to its intrinsic cell adhesion moieties that promote cell spreading and functionality.[20] Here, we adopted a mixture of GelMA and alginate as the bioink,[10] where the alginate component was used to increase the viscosity to achieve a range of bioprinting conditions. The cell-laden bioinks were photo-crosslinked to fix their structures immediately after printing.[10] Detailed investigations of the rheological properties and the printing performance of the GelMA/alginate bioinks can be found in the Supporting Information (Figures S10–S12). We first took advantage of the multibioink printing to design a range of different patterns including a heart-like structure (**Figure 3**A–E), a kidney-like structure (Figure S13A–F, Supporting Information), and stripes with different width (Figure S13G–K, Supporting Information). It was clear that multiple bioinks laden with cells pre-labeled with cell trackers were effectively deposited using our continuous multimaterial bioprinter. The printed structure possessed explicitly separated borders among different cell-laden bioinks (Figure 3B–E, and Figure S13B–F, H–K, Supporting Information). The resolution was determined to be ≈100–200 µm, as indicated from the printed stripe patterns with a range of widths (Figure S13H–K, Supporting Information).

We further printed a pattern of endothelialized tissue, where four sectors of bioinks laden with human dermal fibroblasts (HDFs), HepG2 human hepatocellular cells, human mesenchymal stem cells (hMSCs), and no cells, respectively, were deposited at the base, followed by integration of a pattern on top that resembled the vasculature encapsulating human umbilical vein endothelial cells (HUVECs, Figure 3F). The fluorescence images obtained from different locations clearly revealed successful bioprinting of the desired (cell-laden) bioinks (Figure 3G–I), which laid down the essential basis for future fabrication of complex tissues containing hierarchical assembly of multiple cell types. The cell viability assays, determined immediately and at 1 and 7 d post-bioprinting (Figure 3J and Figure S14A–T, Supporting Information), indicated that all cell types maintained sufficient viability under the UV crosslinking conditions adopted. Comparison with the cells pre-bioprinting (Figure S14A–H vs I–T, Supporting Information) further revealed that the conditions selected for extrusion did not appear to affect cell viability. The cells well spread over a course of 7 d in culture (Figure S14U–X, Supporting Information), indicating the bioactivity provided by the GelMA component of the bioink. The printed endothelialized tissue constructs were further shown to exhibit increased cell proliferation over a period of 3 d analyzed (Figure 3K).

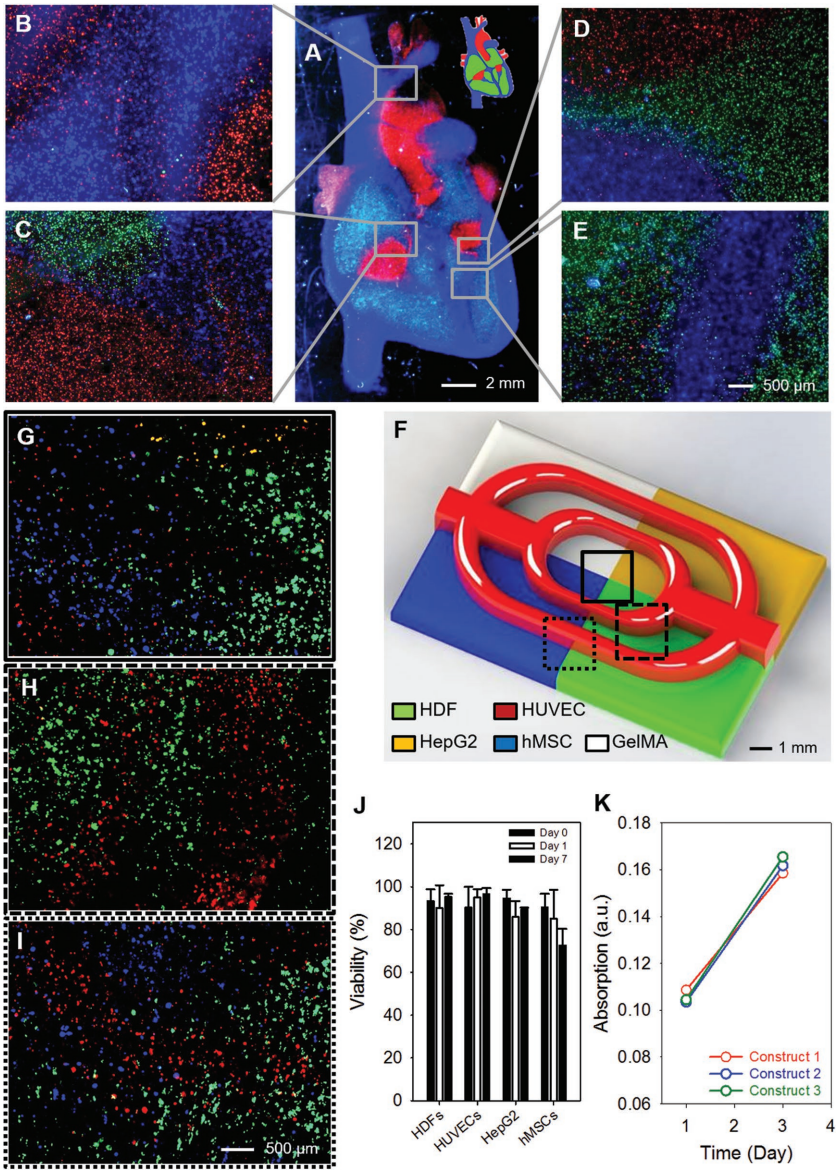

Figure 3. Multimaterial bioprinting of cell-laden structures. A) Fluorescence image showing a printed multi-component heart-like structure. Fluorescent microbeads were used to aid the macroscopic visualization. The inset shows a schematic of the design. B–E) Fluorescence images of different junction regions showing the coexistence of HDFs stained with different cell trackers in the printed cell-embedding construct. F) Schematic showing the design of a vascularized tissue construct containing the four types of cells stained with different cell trackers. G–I) Fluorescence images of different junction regions showing the coexistence of desired cell types in the printed construct. J) Quantification of viability of the four cell types immediately, 1 and 7 d post-bioprinting. K) Proliferation of the cells over a course of 3 d. Printing conditions: 5% GelMA and 1% alginate encapsulating different cells, printhead moving speed = 400 mm min^{-1}, pneumatic pressure = 3 psi.

In addition, we used the multimaterial extrusion bioprinter to generate gradient structures to mimic those occurring in natural tissues, such as the bone. For example, we created a ring-like structure featuring an inward-out gradient in

ADVANCED MATERIALS
www.advmat.de

www.MaterialsViews.com

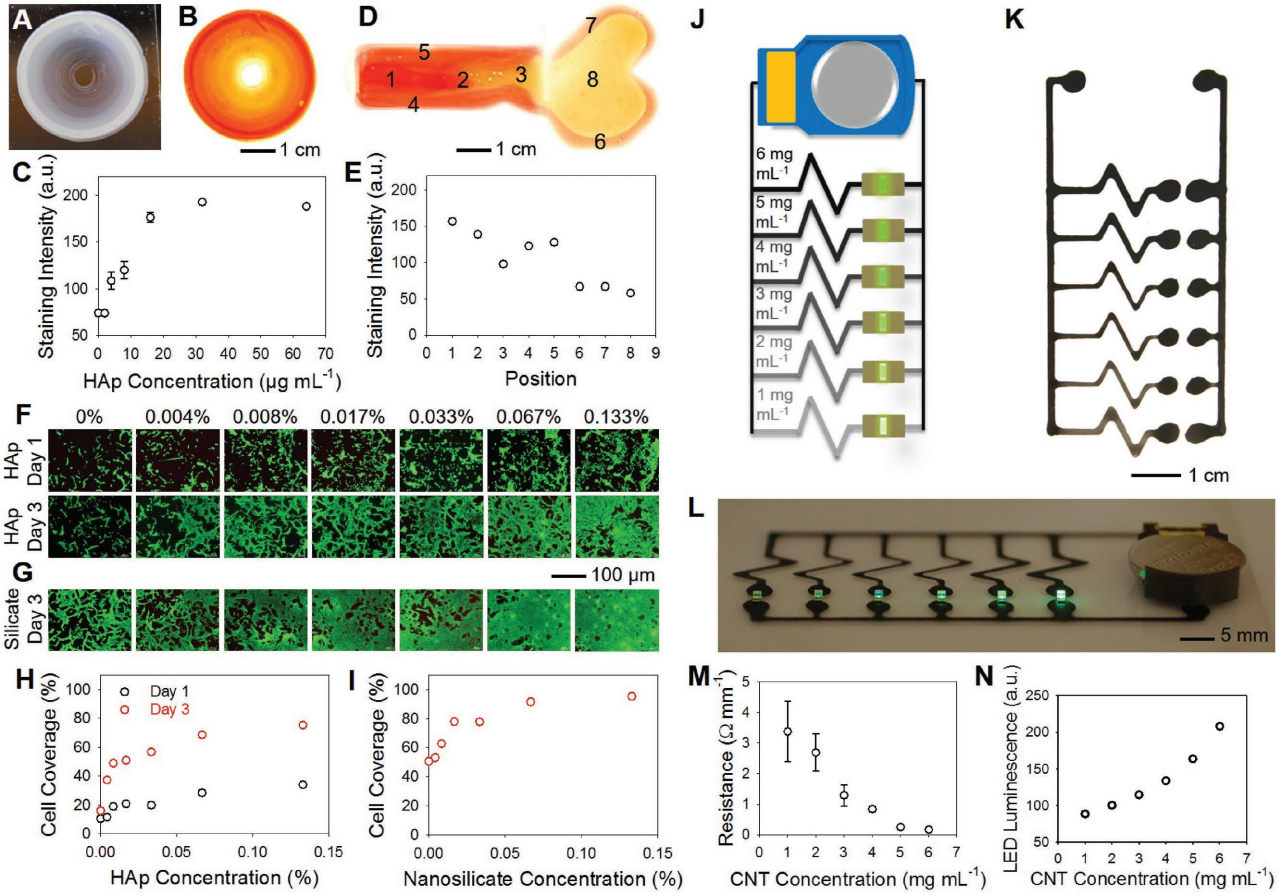

Figure 4. Extended applications of the continuous multimaterial bioprinting platform. A) Printed concentric hydrogel structures containing inward-out gradient of HAp. B) Alizarin Red staining of the same construct revealing the gradient in HAp contents. C) Quantification of the Alizarin Red staining intensities for each ring. D) Printed bone-like structure with desired bioinks containing different concentrations of HAp post-staining with Alizarin Red. E) Quantification of the Alizarin Red staining intensities at selected locations. F,G) Fluorescence image showing the spreading of preosteoblasts on printed hydrogel blocks with gradients of F) HAp and G) nanosilicates. H,I) Quantification of area coverages by the cells on the two substrates with HAp and nanosilicate gradients, respectively. Printing conditions: A–I) 5% GelMA, 2.67% alginate, and 0.5% PI containing various concentrations of HAp and nanosilicates, printhead moving speed = 400 mm min^{-1}, pneumatic pressure = 3 psi. J) Schematic showing the design of the bioelectronic circuit composed of conductive bioinks with a series concentrations of CNTs. K) Photograph of a printed circuit. L) Photograph of a completed circuit where the LEDs showed a series of differential luminescence intensities. M,N) Quantification of the resistance and LED luminescence for bioinks containing different concentrations of CNTs. Printing conditions: 2% alginate containing various concentrations of CNTs, printhead moving speed = 400 mm min^{-1}, pneumatic pressure = 3 psi.

the concentration of hydroxyapatite (HAp) embedded in the GelMA/alginate hydrogel (**Figure 4**A). Alizarin Red staining and quantification of the staining intensities further confirmed the presence of this same type of gradient in HAp contents (Figure 4B,C). Importantly, the shape of the printed constructs containing bioinks with different concentrations of HAp could be arbitrarily controlled to form any desired localized gradients as well as continuous or discrete patterns, as illustrated by our capability to print a bone-shaped hydrogel block (Figure 4D). The Alizarin Red staining indicated that different bioinks containing a range of HAp concentrations were printed across the entire structure, where the same materials (#4 and #5, #6 and #7) printed at discrete locations showed similar staining intensity, revealing reproducible deposition of the bioinks as programmed (Figure 4E).

The printed constructs featuring gradients of inorganic nanoparticles also demonstrated varying bioactivities. Differential attachment and proliferation of MC3T3 preosteoblasts seeded on top of the printed structure containing a gradient of HAp, were observed after 1 and 3 d of culture (Figure 4F,H). The cell seeding efficiency and proliferation were promoted with increasing concentration of HAp. A similar trend in cell behaviors was observed when the preosteoblasts were seeded on printed hydrogels containing a gradient of nanosilicates based on the osteoinductive property of these nanoparticles (Figure 4G,I).[18] This excellent freedom in reliable and smooth switching among selected bioinks during the bioprinting process is critical in recapitulating tissue- and organ-level biomimetic properties, especially when sophisticated structures and/or complex compositions are involved.

Significant interest in bioelectronics is also emerging in biomedicine. A wide range of applications of electronics devices is possible in various fields, including epidermal sensors, soft contact lenses, neurointerfaces, implantable medical devices, and

DOI: 10.1002/adma.201604630

bioactuators.[21] Bioprinting has been increasingly recognized as an excellent technique for depositing conductive bioinks for direct fabrication of bioelectronics, given its convenience, robustness, and cost effectiveness.[22] While many strategies have been developed for printing conductive bioinks, these have been mostly limited by single-ink deposition, which precluded the possibility for the production of complex electronic circuits. Taking advantage of our multimaterial bioprinting platform, we printed a prototype continuous circuit featuring conductive alginate/DNA/carbon nanotube (CNT) bioinks with 1–6 mg mL^{-1} CNTs in parallel (Figure 4J,K, and Movie S8, Supporting Information). This conductive bioink was optimized from our previous formulation used for single-material printing.[23] The printed circuit was completed by attaching a power source (coin battery, 3V) and six miniature green LEDs, which upon connection, exhibited a clear gradient in their luminescence intensity (Figure 4L). The differential luminescence of the LEDs was attributed to the series of resistances (0.17–3.37 Ω mm^{-1}) that the conductive bioinks produced and therefore the difference in the current generated in each parallel unit (Figure 4M,N). Our capability for continuously printing several types of conductive bioinks has paved a new avenue for fabricating complex bioelectronics, where future bioprinting of complex circuits composed of multiple functional electronic units is envisioned.

In summary, we have developed a continuous multimaterial extrusion bioprinting strategy capable of continuously and/or simultaneously depositing up to seven types of bioinks through the integration of a digitally tunable pneumatic single-printhead system, which was able to achieve biofabrication of multicomponent structures at a speed up to 15 times faster than existing nozzle-based modalities. While our demonstrations in the current work are preliminary with limited resolution and functional assays, we primarily aimed to introduce the concept of continuous multimaterial extrusion bioprinting. To this end, we demonstrated the capacity of this platform in bioprinting of sophisticated planar and 3D patterns. In the subsequent proof-of-concept demonstrations, we showed the ability of our bioprinter to produce complex and gradient constructs for applications in tissue engineering and bioelectronics. Notably, our platform may be readily expanded to a large number of channels desired, simply by increasing the numbers of digitally actuated pneumatic valves in the system.

We believe that further optimization in the instrumentation of the bioprinting system will make it a highly efficient modality and a leap forward in the fabrication of physiologically relevant and functional tissues/organs that match the complexity of their in vivo counterparts at clinically relevant speeds. For example, it should be noted that, in the current setup we aligned the individual channels of the printhead side by side, leading to slightly nonconcentric deposition of the multiple bioinks. Nonetheless, the printhead could be further connected to a common outlet, and this different printhead design enabling the materials to mix with different volumes/rates prior to extrusion would further achieve true gradient formation at microscale. The pressure of each channel may also be individually tuned (as to the uniform pressures across different channels in our current system) to allow for dispensing of multiple bioinks with a series of rheological properties. Further optimization of the bioprinter is currently undergoing and will be reported in future publications. We foresee the widespread use of our multimaterial extrusion bioprinting in rapid construction of biomedical devices where a multitude of different materials can be adapted.

Supporting Information

Supporting Information is available from the Wiley Online Library or from the author.

Acknowledgements

W.L., Y.S.Z., and M.A.H. contributed equally to this work as the primary author. The authors acknowledge funding from the National Institutes of Health (AR057837, DE021468, D005865, AR068258, AR066193, EB022403, EB021148), and the Office of Naval Research Presidential Early Career Award for Scientists and Engineers (PECASE). This work was also partially supported by the Fundamental Research Funds for the Central Universities from China (No. 14D310106) and the Tecnológico de Monterrey and MIT Nanotechnology Program. Y.S.Z. acknowledges the National Cancer Institute of the National Institutes of Health Pathway to Independence Award (1K99CA201603-01A1). W.L. further appreciates the financial support from the program of China Scholarships Council (No. 201406630041). J.Y. would like to thank the Australian Endeavour Research Fellowship. M.M.A. and G.T.d.S. gratefully acknowledge funding provided by Gonsejo National de Ciencia y Tecnología (CONACyT; scholarships 262130 and 234713), MIT International Science and Technology Initiatives (MISTI), and Fundación México en Harvard. The authors thank E. Laukaitis for her assistance with the schematic diagram in Figure 1A. The authors also thank R. Steinmeyer, R. Lee, and V. Seksaria for their assistance in hardware/software designs of the printer.

Received: August 29, 2016
Revised: September 23, 2016
Published online:

[1] a) P. Bajaj, R. M. Schweller, A. Khademhosseini, J. L. West, R. Bashir, *Annu. Rev. Biomed. Eng.* **2014**, *16*, 247; b) J. Malda, J. Visser, F. P. Melchels, T. Jüngst, W. E. Hennink, W. J. Dhert, J. Groll, D. W. Hutmacher, *Adv. Mater.* **2013**, *25*, 5011; c) S. V. Murphy, A. Atala, *Nat. Biotechnol.* **2014**, *32*, 773; d) F. Pati, J. Jang, D.-H. Ha, S. W. Kim, J.-W. Rhie, J.-H. Shim, D.-H. Kim, D.-W. Cho, *Nat. Commun.* **2014**, *5*, 3935; e) M. M. Stanton, J. Samitier, S. Sánchez, *Lab Chip* **2015**, *15*, 3111; f) Y. S. Zhang, M. Duchamp, R. Oklu, L. W. Ellisen, R. Langer, A. Khademhosseini, *ACS Biomater. Sci. Eng.* **2016**, *2*, 1710; g) Y. S. Zhang, K. Yue, J. Aleman, K. Moghaddam, S. M. Bakht, V. Dell'Erba, P. Assawes, S. R. Shin, M. R. Dokmeci, R. Oklu, A. Khademhosseini, *Ann. Biomed. Eng.* **2016**.

[2] Y. Yan, X. Wang, Y. Pan, H. Liu, J. Cheng, Z. Xiong, F. Lin, R. Wu, R. Zhang, Q. Lu, *Biomaterials* **2005**, *26*, 5864.

[3] Y. Nahmias, R. E. Schwartz, C. Verfaillie, D. J. Odde, *Biotechnol. Bioeng.* **2005**, *92*, 129.

[4] M. Nakamura, A. Kobayashi, F. Takagi, A. Watanabe, Y. Hiruma, K. Ohuchi, Y. Iwasaki, M. Horie, I. Morita, S. Takatani, *Tissue Eng.* **2005**, *11*, 1658.

[5] U. Demirci, G. Montesano, *Lab Chip* **2007**, *7*, 1139.

[6] a) U. Demirci, G. Montesano, *Lab Chip* **2007**, *7*, 1428; b) J. S. Miller, K. R. Stevens, M. T. Yang, B. M. Baker, D.-H. T. Nguyen, D. M. Cohen, E. Toro, A. A. Chen, P. A. Galie, X. Yu, *Nat. Mater* **2012**, *11*, 768.

[7] a) T. Bhattacharjee, S. M. Zehnder, K. G. Rowe, S. Jain, R. M. Nixon, W. G. Sawyer, T. E. Angelini, *Sci. Adv.* **2015**, *1*, e1500655;

b) C. B. Highley, C. B. Rodell, J. A. Burdick, *Adv. Mater.* **2015**, *27*, 5075; c) T. J. Hinton, Q. Jallerat, R. N. Palchesko, J. H. Park, M. S. Grodzicki, H.-J. Shue, M. H. Ramadan, A. R. Hudson, A. W. Feinberg, *Sci. Adv.* **2015**, *1*, e1500758.
[8] N. Jones, *Nature* **2012**, *487*, 22.
[9] Y.-J. Seol, H.-W. Kang, S. J. Lee, A. Atala, J. J. Yoo, *Eur. J. Cardio-Thorac. Surg.* **2014**, *46*, 342.
[10] C. Colosi, S. R. Shin, V. Manoharan, S. Massa, M. Constantini, A. Barbetta, M. R. Dokmeci, M. Dentini, A. Khademhosseini, *Adv. Mater.* **2015**, *28*, 677.
[11] J. O. Hardin, T. J. Ober, A. D. Valentine, J. A. Lewis, *Adv. Mater.* **2015**, *27*, 3279.
[12] T. J. Ober, D. Foresti, J. A. Lewis, *Proc. Natl. Acad. Sci. USA* **2015**, *112*, 12293.
[13] a) R. Chang, J. Nam, W. Sun, *Tissue Eng., Part A* **2008**, *14*, 41; b) S. Khalil, J. Nam, W. Sun, *Rapid Prototyping J.* **2005**, *11*, 9; c) Z. Yu, Y. Rui, O. Liliang, D. Hongxu, Z. Ting, Z. Kaitai, C. Shujun, S. Wei, *Biofabrication* **2014**, *6*, 035001.
[14] D. B. Kolesky, R. L. Truby, A. S. Gladman, T. A. Busbee, K. A. Homan, J. A. Lewis, *Adv. Mater.* **2014**, *26*, 3124.
[15] a) J. Campbell, I. McGuinness, H. Wirz, A. Sharon, A. F. Sauer-Budge, *J. Nanotechnol. Eng. Med.* **2015**, *6*, 021005; b) T. K. Merceron, M. Burt, Y.-J. Seol, H.-W. Kang, S. J. Lee, J. J. Yoo, A. Atala, *Biofabrication* **2015**, *7*, 035003.
[16] H.-W. Kang, S. J. Lee, I. K. Ko, C. Kengla, J. J. Yoo, A. Atala, *Nat. Biotechnol.* **2016**, *34*, 312.
[17] a) A. K. Gaharwar, R. K. Avery, A. Assmann, A. Paul, G. H. McKinley, A. Khademhosseini, B. D. Olsen, *ACS Nano* **2014**, *8*, 9833; b) B. Ruzicka, E. Zaccarelli, *Soft Matter* **2011**, *7*, 1268.
[18] A. K. Gaharwar, S. M. Mihaila, A. Swami, A. Patel, S. Sant, R. L. Reis, A. P. Marques, M. E. Gomes, A. Khademhosseini, *Adv. Mater.* **2013**, *25*, 3329.
[19] L. E. Bertassoni, J. C. Cardoso, V. Manoharan, A. L. Cristino, N. S. Bhise, W. A. Araujo, P. Zorlutuna, N. E. Vrana, A. M. Ghaemmaghami, M. R. Dokmeci, *Biofabrication* **2014**, *6*, 024105.
[20] a) J. W. Nichol, S. T. Koshy, H. Bae, C. M. Hwang, S. Yamanlar, A. Khademhosseini, *Biomaterials* **2010**, *31*, 5536; b) K. Yue, G. Trujillo-de Santiago, M. M. Alvarez, A. Tamayol, N. Annabi, A. Khademhosseini, *Biomaterials* **2015**, *73*, 254.
[21] a) A. M. Gaikwad, G. L. Whiting, D. A. Steingart, A. C. Arias, *Adv Mater.* **2011**, *23*, 3251; b) D.-H. Kim, N. Lu, R. Ghaffari, J. A. Rogers, *NPG Asia Mater.* **2012**, *4*, 15; c) F. Garnier, R. Hajlaoui, A. Yassar, P. Srivastava, *Science* **1994**, *265*, 1684; d) X. Duan, T. M. Fu, J. Liu, C. M. Lieber, *Nano Today* **2013**, *8*, 351.
[22] a) J. T. Muth, D. M. Vogt, R. L. Truby, Y. Menguc, D. B. Kolesky, R. J. Wood, J. A. Lewis, *Adv. Mater.* **2014**, *26*, 6307; b) E. B. Secor, S. Lim, H. Zhang, C. D. Frisbie, L. F. Francis, M. C. Hersam, *Adv. Mater.* **2014**, *26*, 4533.
[23] S. R. Shin, R. Farzad, A. Tamayol, V. Manoharan, P. Mostafalu, Y. S. Zhang, M. Akbari, S. M. Jung, D. Kim, M. Commotto, N. Annabi, F. E. Al-Hazmi, M. R. Dokmeci, A. Khademhosseini, *Adv. Mater.* **2016**, *28*, 3280.

Adv. Mater. **2016**,
DOI: 10.1002/adma.201604630